JACS
JOURNAL OF THE AMERICAN CHEMICAL SOCIETY
Article
pubs.acs.org/JACS

Reactivity of Atomic Oxygen Radical Anions Bound to Titania and Zirconia Nanoparticles in the Gas Phase: Low-Temperature Oxidation of Carbon Monoxide

Jia-Bi Ma,[†,‡,§] Bo Xu,[†,‡] Jing-Heng Meng,[†,‡] Xiao-Nan Wu,[†] Xun-Lei Ding,[†] Xiao-Na Li,[†] and Sheng-Gui He*[,†]

[†]Beijing National Laboratory for Molecular Sciences, State Key Laboratory for Structural Chemistry of Unstable and Stable Species, Institute of Chemistry, Chinese Academy of Sciences, Beijing 100190, P.R. China

[‡]University of Chinese Academy of Sciences, Beijing 100049, P.R. China

[§]Institut für Chemie, Technischen Universität Berlin, Strasse des 17. Juni 135, 10623 Berlin, Germany

Supporting Information

ABSTRACT: Titanium and zirconium oxide cluster anions with dimensions up to nanosize are prepared by laser ablation and reacted with carbon monoxide in a fast low reactor. The cluster reactions are characterized by time-of-flight mass spectrometry and density functional theory calculations. The oxygen atom transfers from $(TiO_2)_nO^-$ (n = 3−25) to CO and formations of $(TiO_2)_n^-$ are observed, whereas the reactions of $(ZrO_2)_nO^-$ (n = 3−25) with CO generate the CO addition products $(ZrO_2)_nOCO^-$, which lose CO_2 upon the collisions (studied for n = 3−9) with a crossed helium beam. The computational study indicates that the $(MO_2)_nO^-$ (M = Ti, Zr; n = 3−8) clusters are atomic radical anion (O^-) bonded systems, and the energetics for CO oxidation by the O^- radicals to form CO_2 is strongly dependent on the metals as well as the cluster size for the titanium system. Atomic oxygen radical anions are important reactive intermediates, while it is difficult to capture and characterize them for condensed phase systems. The reactivity pattern of the O^--bonded $(TiO_2)_nO^-$ and $(ZrO_2)_nO^-$ correlates very well with different behaviors of titania and zirconia supports in the low-temperature catalytic CO oxidation.

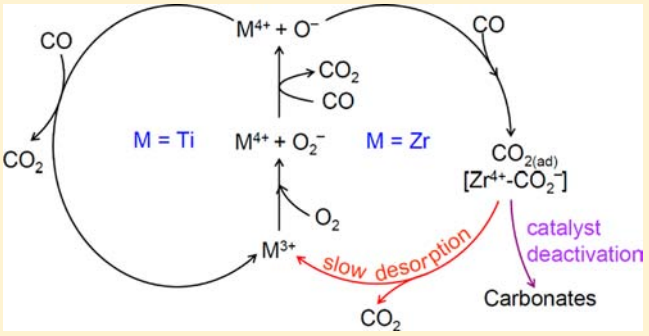

1. INTRODUCTION

Low-temperature oxidation of carbon monoxide by molecular oxygen has quite a few potential applications, such as air purification, pollution control, and fuel gas cleanup.[1] For example, titania-supported gold is well-known to catalyze CO oxidation at temperatures down to −60 °C.[2] This catalytic system along with other closely related ones (e.g., Au/ZrO_2, Au/CeO_2, etc.)[3−7] has been studied for decades in order to understand the molecular origin of its high activity. However, the mechanistic details and the nature of active sites as well as support effects that have been proposed by different investigations are often controversial.[4c] As to the low-temperature CO oxidation by O_2 over Au/TiO_2 or other catalysts such as Co_3O_4,[1b] it is agreed upon that reactive oxygen species (ROS) are involved.[1,4−8] Superoxide radicals (O_2^-), peroxide species (O_2^{2-}), and atomic oxygen radical anions (O^-) are three typical ROS that are generally proposed as intermediates in the O_2 activation and dissociation process: $O_2 \rightarrow O_2^- \rightarrow O_2^{2-} \rightarrow O^- \rightarrow O^{2-}$.[9]

The superoxide and peroxide species have been identified to be involved in the low-temperature CO oxidation over Au/TiO_2[7] and related systems[6] by Raman, infrared, and/or electron spin resonance spectroscopic methods. In sharp contrast, so far there is no convincing evidence for the involvement of atomic oxygen radical anions in catalytic reactions, although one would expect that the reaction of O_2^- with CO under participation of gold[10] can generate O^-:

$$O_2^- + CO \xrightarrow{Au} O^- + CO_2 \quad (1)$$

Furthermore, the generated O^- together with the redox couple Ti^{4+}/Ti^{3+} can oxidize a second CO molecule over Au/TiO_2:

$$O^- + CO + Ti^{4+} \rightarrow CO_2 + Ti^{3+} \quad (2)$$

In this study, we report good experimental evidence to support the above hypothesis.

Recently, it has been demonstrated that the study of metal oxide clusters[11] in the gas phase under well-controlled conditions provides an alternative way to reveal mechanistic details involved with the surface chemistry of ROS, especially for the highly reactive O^- radicals,[12] which may have too short lifetimes and too low concentrations to be effectively

Received: May 9, 2012
Revised: November 30, 2012
Published: January 31, 2013

characterized in condensed-phase systems.[9a,13] The reaction between CO and the free O^- anion in the gas phase has been well-studied:[14]

$$O^- + CO \rightarrow CO_2 + e^- \quad (3)$$

In this work, the titanium and zirconium oxide cluster anions $(MO_2)_nO^-$ (M = Ti, Zr; n = 3−25) with dimensions up to a nanosize[15] are prepared and reacted with CO in the gas phase in order to uncover the mechanisms that are operative at a molecular level. Previously, it had been suggested that charge transfer between gold and the oxide support under oxidative (working) conditions generates positively charged gold and negatively charged oxide species.[16] Recently, convincing evidence has been provided that in the oxidation of CO over Au/TiO_2 and Au/ZrO_2 catalysts, the titania and zirconia supports participate directly in the reaction by supplying active oxygen species at the perimeter of the gold−oxide interface.[4] Moreover, well comparative studies indicated that Au/TiO_2[2] and Au/ZrO_2[5] catalysts behave quite differently in the CO oxidation; for example, the former is superior to the latter in terms of activity and stability. Thus, the study of free, unsupported titanium and zirconium oxide cluster anions serves as a first step to interpret support effects that have been extensively studied for the catalytically active Au/TiO_2 and Au/ZrO_2 systems.[2,4a,5,17] While titanium and zirconium oxide clusters have been extensively studied,[18−20] the gas-phase reactivity of nanosized systems has not yet been explored experimentally.

2. METHODS

2.1. Experimental Methods. The details of the experimental setup can be found in the previous studies,[12e,20b] and only a brief outline of the experiments is given below. The $M_xO_y^-$ clusters (M = Ti, Zr) are produced by laser ablation of a Ti (Zr) disk in the presence of 1% N_2O seeded in He carrier gas. The so-generated clusters react in a downstream fast-flow reactor with pulsed-in gases (10% CO or N_2 in He) for about 60 μs. Before pulsing the prepared gases (N_2O/He, CO/He, and N_2/He) into the vacuum system, it is useful to pass them through copper tube coils at low-temperature (~200 K, dry ice in ethanol) in order to remove a trace amount of water from the gas handling system. The instantaneous total gas pressure in the reactor is around 220 Pa at T = 298 K and this corresponds to a collisional rate of about 5×10^7 s^{-1}.[20b] The intracluster vibrations are equilibrated to close to room-temperature before reacting with diluted CO.[12e,20b] The reactant and product ions exiting from the reactor are detected by either a high-resolution reflectron time-of-flight mass spectrometer (TOF-MS)[12e] or a separate TOF/TOF-MS for collision-induced dissociation (CID). The mass resolution of the secondary TOF-MS employed in this work for the CID has been improved from the previous one[20b] by using two identical reflectors with a Z-shaped configuration.

2.2. Computational Methods. Density functional theory (DFT) calculations with the hybrid B3LYP[21] functional and the Gaussian 03 program[22] are performed to study the structures of $(MO_2)_nO^-$ (M = Ti, Zr and n = 3−8) clusters. Metal oxide clusters with more than 10 atoms can have a high number of possible geometries. A Fortran code based on a genetic algorithm (GA) is developed and tested to well reproduce the global minimum (GM) structure of $Al_8O_{12}^+$ in the literature.[23] Such a code is used to generate initial guess structures of $(TiO_2)_nO^-$ and $(ZrO_2)_nO^-$ (n = 4−8). For each cluster, the smaller LanL2DZ basis sets[24] are adopted for Ti, Zr, and O atoms in the GA calculations that produce more than 200 optimized structures, among which more than 20 of the low-lying isomers are reoptimized by employing the larger TZVP basis sets[25] for Ti and O atoms and a D95V basis set combined with the Stuttgart/Dresden relativistic effective core potential[26] (denoted as SDD in Gaussian software) for Zr atoms. The results reported in this work are all from B3LYP calculations with basis sets of TZVP for Ti and O (as well as C and H, see below) and SDD for Zr and Au.

The DFT calculations are also performed for the detailed reaction mechanisms of $Ti_3O_7^- + CO \rightarrow Ti_3O_6^- + CO_2$ and $HAu_2TiO_4 + CO \rightarrow HAu_2TiO_3 + CO_2$. This involves geometry optimizations of reaction intermediates and transition states (TSs) for which the Berny algorithm[27] is adopted. Intrinsic reaction coordinate calculations[28] are also performed so that a TS connects two appropriate local minima. The variational transition state theory (VTST)[29] is used to calculate the rate constants for CO_2 desorption from $(MO_2)_nOCO^-$ (M = Ti, Zr and n = 3−5) intermediates that carry vibrational energies of $(MO_2)_nO^-$ and CO (E_{vib}), center-of-mass kinetic (E_k), and binding energies (E_b) between $(MO_2)_nO^-$ and CO. The E_{vib} and E_b are taken from the DFT calculations and $E_k = \mu v^2/2$, in which μ is the reduced mass and v is the cluster beam velocity (≈1 km/s). The VTST calculations involve geometry optimizations of $(MO_2)_nOCO^-$ by fixing the distance between $(MO_2)_n$ and CO_2 moieties at various values. The density and number of states required for VTST calculations are obtained with direct count method[30] by using the DFT-calculated vibrational frequencies under approximation of harmonic vibrations (see ref 31 for details).

3. RESULTS

3.1. Experimental Results. Selected TOF mass spectra for interactions of the laser ablation generated $Ti_xO_y^-$ and $Zr_xO_y^-$ with CO in the reaction cell are shown in Figure 1 (see Figures S1 and S2 in the Supporting Information for complete spectra). Both titanium and zirconium have several stable isotopes. The experimentally observed isotopic patterns of $Ti_5O_{11}^-$ (Figure 1b) and $Zr_4O_9^-$ (Figure 1f) agree with the simulated ones (Figure 1a,e) very well, indicating that the H_2O adsorption that often occurs in the distributions of metal oxide clusters[12a,32] is negligible in this work. Upon the interaction with CO in the reactor (Figure 1c,g), the signal magnitudes of $Ti_5O_{11}^-$ and $Zr_4O_9^-$ clusters decrease significantly, while those of the more

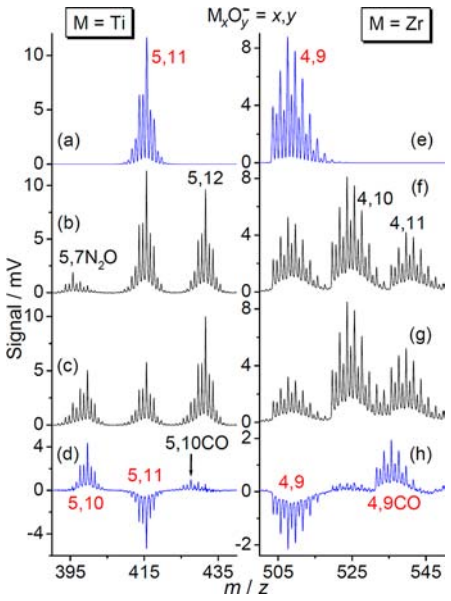

Figure 1. Selected TOF mass spectra for reactions of $Ti_5O_y^-$ (c) and $Zr_4O_y^-$ (g) with 1.4 and 0.6 Pa CO in the reaction cell, respectively. The complete spectra are given in Figures S1 and S2 (Supporting Information). The numbers x,y denote $M_xO_y^-$ in which M = Ti (left) or Zr (right). The reference spectra with N_2 in the reactor (b, f), the difference spectra (d = c − b, h = g − f), and the simulated $Ti_5O_{11}^-$ and $Zr_4O_9^-$ isotopomers (a, e) are shown.

dx.doi.org/10.1021/ja311695t | J. Am. Chem. Soc. 2013, 135, 2991−2998

oxygen-rich clusters $Ti_5O_{12}^-$ and $Zr_4O_{10,11}^-$ do not change within the experimental uncertainties. The difference spectrum of Figure 1d (spectrum of Figure 1c minus the one of Figure 1b) clearly shows that the main part of the signal depletion of $Ti_5O_{11}^-$ results in the signal appearance of $Ti_5O_{10}^-$. In sharp contrast, the signal depletion of $Zr_4O_9^-$ results in the signal appearance of $Zr_4O_9CO^-$ rather than $Zr_4O_8^-$ (Figure 1h).

It turns out that the reactivity patterns of $(TiO_2)_nO^-$ (n = 3–25) and $(ZrO_2)_nO^-$ (n = 3–25) cluster series (difference spectra shown in Figure 2 for n = 10–20) are very similar to

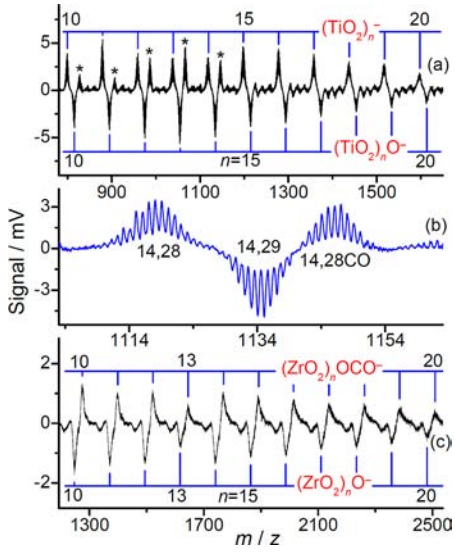

Figure 2. The difference spectra (similar to d and h in Figure 1) for reactions of $Ti_{10-20}O_y^-$ (a) and $Zr_{10-20}O_y^-$ (c) with CO. Peaks marked with asterisks in spectrum a can be assigned as $(TiO_2)_nCO^-$ (n = 10–14). A portion of the spectrum in a is expanded and shown (b).

those of $Ti_5O_{11}^-$ and $Zr_4O_9^-$, respectively. The experiments thus suggest channels of oxygen atom transfer (eq 4) and CO adsorption (eq 5) over titanium and zirconium oxide systems, respectively:

$$(TiO_2)_nO^- + CO \rightarrow (TiO_2)_n^- + CO_2 \quad (n = 3–25) \tag{4}$$

$$(ZrO_2)_nO^- + CO \rightarrow (ZrO_2)_nOCO^- \quad (n = 3–25) \tag{5}$$

Note that the above reactions may also take place over further larger $(MO_2)_nO^-$ (M = Ti, Zr; n > 25) clusters (Figures S1 and S2, Supporting Information), while the experimental identification suffers from low abundances of these nanoparticles[15] in the cluster source. The CO association products of $(ZrO_2)_nOCO^-$ (n = 3–9) are mass-selected and characterized by subjecting them to CID. The evaporation of CO_2 (eq 6) dominates the CID spectra (see Figure S3 of the Supporting Information for examples), which suggests that reaction 5 corresponds to an oxidative adsorption of CO molecules on the zirconium oxide clusters:

$$(ZrO_2)_nOCO^- \xrightarrow{\Delta(\text{CID with He})} (ZrO_2)_n^- + CO_2 \quad (n = 3–9) \tag{6}$$

It is noteworthy that for titanium series $(TiO_2)_nO^-$, only the $Ti_4O_9^-$ (n = 4) cluster can pick up CO in the reaction cell to form the CO association product $Ti_4O_9CO^-$ (Figure S1, Supporting Information). However, loss of CO rather than CO_2 is observed in the CID of $Ti_4O_9CO^-$ (Figure S3, Supporting Information). In addition, the $Ti_4O_{10}^-$ and $(TiO_2)_n^-$ (n = 3–14) clusters can also pick up the CO molecules (Figures 2 and S1, Supporting Information). The formation of these CO association products can be due to relatively strong Ti–CO interaction, which is not the main topic of this study, and a brief interpretation is given in the Supporting Information.

The pseudo-first-order rate constants (k_1) for the cluster reactions in fast-flow reactor can be estimated[31] and the k_1 values for reactions 4 and 5 are on the order of 10^{-11} cm^3 molecule^{-1} s^{-1}. For example, $k_1(Ti_5O_{11}^-+CO)$ and $k_1(Zr_5O_{11}^-+CO)$ are about 3×10^{-11} and 7×10^{-11} cm^3 molecule^{-1} s^{-1}, respectively. By using the hard sphere[33] and classical[34] average dipole orientation (ADO) theories, the theoretical rates of collisions (k_{ADO}) between $Ti_5O_{11}^-$ and CO can be calculated to be 7.3×10^{-10} and 6.9×10^{-10} cm^3 molecule^{-1} s^{-1}, respectively. The reaction efficiency (k_1/k_{ADO}) of $Ti_5O_{11}^-$ with CO is around 4%. Similarly, the efficiency is estimated to be 10% for the reaction of $Zr_5O_{11}^-$ with CO.

3.2. Computational Results. The DFT-calculated lowest-lying isomeric structures of $(MO_2)_nO^-$ (M = Ti, Zr and n = 3–8) are shown in Figure 3, and the information on low-lying

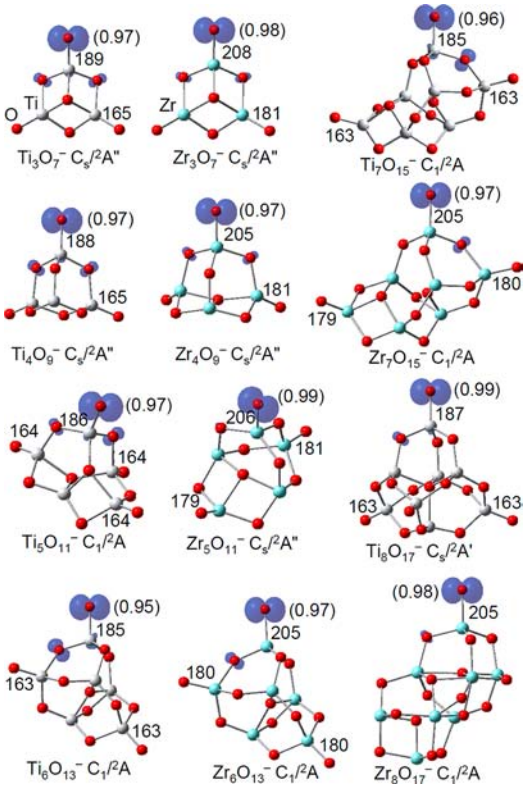

Figure 3. DFT calculated structures and unpaired spin density distributions for the lowest-lying isomers of $(MO_2)_nO^-$ (M = Ti, Zr; n = 3–8). Bond lengths (in pm) and unpaired spin densities (in μ_B and in the parentheses) on the oxygen atoms are shown.

isomers for each of the $n \geq 4$ clusters is given in Figures S4–S13 (Supporting Information). The structures of $Ti_3O_7^-$, $Zr_3O_7^-$, and $Zr_4O_9^-$ have been reported previously.[18b,21,35] The lowest-lying isomer of $Zr_4O_9^-$ reported here differs only slightly from the one of ref 18b, where a structure similar to IS2 in Figure S9 (Supporting Information) was given. As shown in Figure 3, the topological stucutures of $(TiO_2)_nO^-$ and

dx.doi.org/10.1021/ja311695t | J. Am. Chem. Soc. 2013, 135, 2991–2998

$(ZrO_2)_nO^-$ are identical at n = 3, 6, and 7 or similar to each other at n = 4 and 5. The DFT studied largest (n = 8) clusters $Ti_8O_{17}^-$ and $Zr_8O_{17}^-$ have very different lowest-lying structures: the former (close to C_{3v} symmetry) has four Ti−O terminal bonds, while the latter is more compact and has only one Zr−O terminal bond. Each of the structures shown in Figure 3 contains one oxygen atom that possesses an unpaired spin density (UPSD) value of about 1 μ_B located on one O_{2p} orbital. These oxygen atoms have essentially the same UPSD distributions as the free O^- anion. The UPSD distributions for almost all of the low-lying cluster isomers in Figures S4−S13 (Supporting Information) are also similar: one of the O atoms in each isomer has the UPSD of about 1 μ_B. As a result, the $(TiO_2)_{3-8}O^-$ and $(ZrO_2)_{3-8}O^-$ clusters are atomic oxygen radical anion bounded particles.

The detailed mechanism for the reaction of CO with the cluster bonded O^- radical anion is studied for $Ti_3O_7^-$ + CO (Figure 4a). An encounter complex (IM1) with a small binding energy (0.04 eV) is located. Further approach of CO to the O^- radical that leads to oxidation of CO to CO_2^-, and formation of the intermediate IM2 is facile. The oxidation process ($CO + O^- \rightarrow CO_2^-$) releases a large amount of energy (1.67 eV) that drives the desorption of a CO_2 molecule from the reaction complex (IM2 → IM3 → $Ti_3O_6^-$ + CO_2). It is noteworthy that the IM1 and TS1 in Figure 4a are probably not real species, because they are of the energy of the van der Waals clusters and may not be properly described by the DFT calculations.

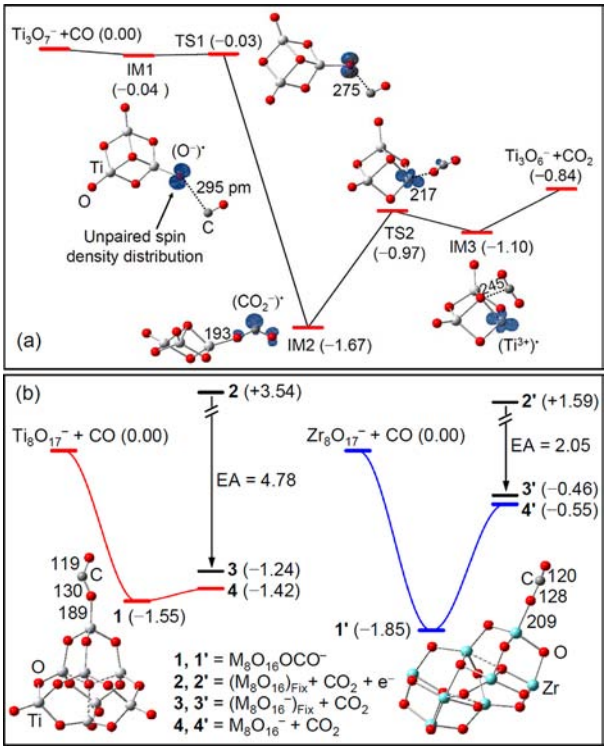

Figure 4. DFT calculated (a) reaction pathway for $Ti_3O_7^-$ + CO → $Ti_3O_6^-$ + CO_2 and (b) simplified potential energy profiles for oxidative CO absorption and CO_2 desorption in the reactions of CO with $M_8O_{17}^-$ (M = Ti, Zr). Bond lengths are in picometers. The zero-point vibration corrected energies (ΔH_{0K} in eV) of the reaction intermediates (IM1−IM3; **1** and **1′**), transition states (TS1 and TS2), and products ($Ti_3O_6^-$ +CO_2; **4** and **4′**) with respect to the separated reactants are given. The energies of **2**/**3** and **2′**/**3′** are calculated with the geometric parameters of M_8O_{16} being fixed at the values of the M_8O_{16} moiety in **1** and **1′**, respectively.

The DFT calculations are also performed to optimize the structures of the reaction complexes $(MO_2)_nOCO^-$ (such as IM2 in Figure 4a) that correspond to oxidative adsorption of CO onto the lowest-lying isomers of $(MO_2)_nO^-$ in Figure 3, and the energetics involved are listed in Table 1 and shown in Figure 4b for a comparison of $Ti_8O_{17}^-$ + CO with $Zr_8O_{17}^-$ + CO reaction systems. The second column of Table 1 indicates that energies released in the oxidative CO adsorption are similar for both the Ti (1.5−1.7 eV) and Zr (1.7−1.8 eV) systems. While the oxidations of CO by both $(TiO_2)_nO^-$ and $(ZrO_2)_nO^-$ to form CO_2 are exothermic ($\Delta H_{Total} < -0.5$ eV, see the third column of Table 1), they differ largely with regard to the desorption of CO_2, which is generally much more difficult to achieve from $(ZrO_2)_nOCO^-$ ($\Delta H_{D\text{-}CO2} \geq 0.96$ eV, see the fourth column of Table 1 and Figure 4b) as compared with $(TiO_2)_nOCO^-$ ($\Delta H_{D\text{-}CO2} \leq 0.83$ eV). In each of the CO adsorption complexes of $(TiO_2)_{3-8}OCO^-$ and $(ZrO_2)_{3-8}OCO^-$ (such as IM2, **1** and **1′** in Figure 4), the CO_2 unit has a bent bond angle (∠O−C−O = 132°−134°) and UPSD of about 1 μ_B, so the CO_2 moiety is the CO_2^- radical anion, which is tightly bonded in the cluster species (see the fifth column of Table 1). During the desorption of CO_2 from $(MO_2)_nOCO^-$, the net charge (e^-) of CO_2^- is transferred to the $(MO_2)_n$ moiety to reduce one of the M^{4+} (M = Ti or Zr) ions to M^{3+} [see Figure 4a for Ti^{4+} + e^- (IM2) → Ti^{3+} (IM3)]. The orbital analysis (Figures S15 and S16, Supporting Information) finds that in the process of $(MO_2)_n$ + e^- → $(MO_2)_n^-$, the electron fills into the lowest unoccupied molecular orbital (LUMO) of $(MO_2)_n$ that is primarily composed of one $3d_{z^2}$(M=Ti) or one $4d_{z^2}$(M=Zr) atomic orbital. Because the energy of $3d_{z^2}$ is lower than that of $4d_{z^2}$ (see the LUMO energies in the ninth column of Table 1), the electron affinities (EAs) of $(TiO_2)_n$ are all higher than those of $(ZrO_2)_n$ for n = 3−8 (see the sixth column of Table 1 and notes in ref 36). As a result, the desorption of CO_2 can be much more difficult from $(ZrO_2)_nOCO^-$ than from $(TiO_2)_nOCO^-$ (see Figure 4b for one example). The seventh column of Table 1 indicates that due to larger EAs of $(TiO_2)_n$ versus $(ZrO_2)_n$, the relaxation energies of the former are also slightly higher than that of the latter, which further favors the CO_2 desorption from $(TiO_2)_nOCO^-$ rather than from $(ZrO_2)_nOCO^-$ (compare **3**→**4** with **3′**→**4′** in Figure 4b).

The rate constants (k_d) for CO_2 desorption from $(MO_2)_nOCO^-$ (M = Ti, Zr; n = 3−5) intermediates are estimated with the VTST calculations[29] and the results are listed in Table 2. The k_d values of $(TiO_2)_nOCO^-$ are large (10^8−10^{11} s^{-1}) while those of $(ZrO_2)_nOCO^-$ are much smaller (10^5−10^7 s^{-1}). As the rate of collision between the clusters and He bath gas amounts to 5 × 10^7 s^{-1} (see Methods), the $(ZrO_2)_nOCO^-$ intermediates can be collisionally stabilized[37] in contrast to $(TiO_2)_nOCO^-$, which will rather dissociate into $(TiO_2)_n^-$ and CO_2. We note that the DFT-calculated energetics and the estimated rate constants (k_d) are in good agreement with the experimental results [reaction 4 versus 5; loss of CO_2 from $(ZrO_2)_nOCO^-$ in the CID, reaction 6].

4. DISCUSSION

4.1. Importance of Studying Large-Sized Transition Metal Oxide Clusters. The reactivity of transition metal oxide (TMO) clusters[11] is actively studied in order to understand molecular level mechanisms of catalytic processes over related

Table 1. DFT Calculated Energies (in eV) for $(MO_2)_nO^-$ + CO (M = Ti, Zr)[a]

1	2	3	4	5	6	7	8	9
n	$\Delta H_{A\text{-}CO}$[b]	ΔH_{Total}[b]	$\Delta H_{D\text{-}CO2}$[b]	ΔE[c]	ΔE_{EA}[c]	ΔE_{Relax}[c]	ΔE_{ADE}[b]	E_{LUMO}[d]
				M = Ti				
3	−1.67	−0.84	0.83	4.02	3.10	0.09	3.02	−4.78
4	−1.66	−1.28	0.38	3.82	3.10	0.34	3.27	−4.68
5	−1.53	−1.21	0.32	4.60	4.13	0.15	4.00	−5.67
6	−1.54	−1.24	0.30	4.29	3.84	0.15	3.32	−5.27
7	−1.52	−1.34	0.28	4.39	3.93	0.18	3.06	−5.31
8	−1.55	−1.42	0.13	5.09	4.78	0.18	4.64	−6.14
				M = Zr				
3	−1.78	−0.60	1.18	4.13	2.94	0.01	2.74	−4.51
4	−1.72	−0.63	1.09	4.11	2.99	0.03	2.40	−4.53
5	−1.78	−0.76	1.02	3.74	2.68	0.04	2.40	−4.16
6	−1.71	−0.70	1.01	4.41	3.34	0.06	3.14	−4.83
7	−1.70	−0.74	0.96	4.34	3.32	0.06	2.59	−4.79
8	−1.85	−0.55	1.30	3.44	2.05	0.09	1.60	−3.41

[a]Columns are numbered for easy reference to the text discussion. [b]Enthalpy changes for $(MO_2)_nO^- + CO \rightarrow (MO_2)_nOCO^-$ ($\Delta H_{A\text{-}CO}$), $(MO_2)_nO^- + CO \rightarrow (MO_2)_n^- + CO_2$ (ΔH_{Total}), $(MO_2)_nOCO^- \rightarrow (MO_2)_n^- + CO_2$ ($\Delta H_{D\text{-}CO2}$), and $(MO_2)_n^- \rightarrow (MO_2)_n + e^-$ (ΔE_{ADE}) at T = 0 K. [c]Energy differences between $[(MO_2)_n]_{Fix} + CO_2 + e^-$ and $(MO_2)_nOCO^-$ (ΔE), $[(MO_2)_n]_{Fix} + e^-$ and $[(MO_2)_n^-]_{Fix}$ (ΔE_{EA}), and $[(MO_2)_n^-]_{Fix}$ and $(MO_2)_n^-$ (ΔE_{Relax}). The geometric parameters of $[(MO_2)_n]_{Fix}$ and $[(MO_2)_n^-]_{Fix}$ are fixed at the values of the $(MO_2)_n$ moiety in $(MO_2)_nOCO^-$. See Figure 4 for examples of the $(MO_2)_nOCO^-$ structures (IM2, **1**, and **1′**). [d]Energy of the lowest unoccupied molecular orbital of neutral $[(MO_2)_n]_{Fix}$.

Table 2. Estimated Rate Constants (in s^{-1}) for CO_2 Desorption[a]

	clusters (T = 298 K)[b]			bulk[c]		
1	2	3	4	5	6	7
	n = 3	n = 4	n = 5	T = 230 K	T = 298 K	T = 418 K
Ti	1.9×10^8	3.6×10^{11}	3.1×10^{10}	$>10^{12}$	$>10^{12}$	$>10^{12}$
Zr	1.1×10^7	5.6×10^6	6.0×10^5	1.2×10^{-10}	3.6×10^{-4}	70

[a]Columns are numbered for easy reference to the text discussion. [b]From VTST calculations for $(MO_2)_nOCO^- \rightarrow (MO_2)_n^- + CO_2$ (M = Ti, Zr); see Computational Methods. [c]Calculated with $(k_BT/h)e^{-\Delta G/k_BT}$, in which ΔG is free energy barrier, and k_B and h are the Boltzmann and Plank constants, respectively. The ΔG is estimated by the DFT-calculated Gibbs free energy difference between $M_8O_{16}^- + CO_2$ and $M_8O_{16}OCO^-$ (see Figure 4b for structures). The ΔG values for zirconium species at T = 230, 298, and 418 K are 1.03, 0.96, and 0.84 eV, respectively. These energies are negative (−0.14 to ca.−0.33 eV) for titanium species.

bulk oxides. The TMO clusters with oxygen-centered radicals (the O^- radical anion)[12] are able to oxidize various small molecules[12,38] including CO[18,20b,39] efficiently under thermal collision conditions. This result is in contrast with the fact that the studied TMO clusters without the O^- centers are usually inert under the same experimental conditions,[12a,e,20,38c−e,39c] indicating the importance of oxygen-centered radicals in the low-temperature oxidation reactions. However, most of the TMO clusters studied are small, typically with three to five metal atoms. Researchers of cluster sciences as well as other related areas such as practical catalysis should care very much about one important question: is the chemistry of oxygen-centered radicals from study of small clusters really applicable for interpretation of bulk materials or at least nanoparticles? This study of large titanium and zirconium oxide clusters with a nanosize[15] is making an effort to address this question.

The experiments have provided experimental data for $(MO_2)_nO^-$ (M = Ti, Zr) clusters with n = 3−25. Note that with the densities of bulk titania and zirconia, the diameters of $Ti_{25}O_{51}^-$ and $Zr_{25}O_{51}^-$ are 1.15 and 1.20 nm, respectively.[15] The computations (Figure 3) interpreted that the reactivity pattern observed (reactions 4−6) are due to the oxidation of CO by the cluster bonded O^- radical anions for $(MO_2)_nO^-$ clusters with n = 3−8. It is very difficult at present to determine the reliable global minimum structures for further larger $(MO_2)_nO^-$ (n > 8) clusters. However, on the basis of the results that all of the lowest-lying (Figure 3) and the majority of low-lying isomers (Figures S4−S13, Supporting Information) of $(MO_2)_{3-8}O^-$ contain O^- radicals, it is reasonable to propose that the reactivity of large $(MO_2)_nO^-$ clusters (n > 8) is also due to the presence of these structural motifs. An overall positive answer to the important question (applicability of small cluster chemistry) is fortunately reached with the present study.

Although there is an overall positive answer to the above question, the fourth column of Table 1 tells that the energetics data for large and small titanium cluster systems can be very different: desorption of CO_2 from $Ti_8O_{16}OCO^-$ requires much smaller energy (0.13 eV) than that from $Ti_3O_6OCO^-$ (0.83 eV). As the cluster size increases (n = 3 → 8), the energy decrease for desorption of CO_2 from $(TiO_2)_nOCO^-$ is correlated with the general increase of the electron affinity of $(TiO_2)_n$ (ΔE_{EA}, the sixth column of Table 1). While the ΔE_{EA} values in this work are calculated with the unrelaxed structures of the $(MO_2)_n$ moieties in $(MO_2)_nOCO^-$, these theoretical electron binding energies of $(TiO_2)_n$ are in good agreement with the photoelectron spectroscopy (PES) determined vertical electron detachment energies (VDEs) of $(TiO_2)_n^-$ by Zhai and Wang:[19b] the experimental VDEs of $(TiO_2)_n^-$ increases from 3.15 eV at n = 3 to 4.70 eV at n = 8. The relative positions of the Ti 3d and O 2p derived bands as well as the energy gaps measured from the PES study of $(TiO_2)_n^-$ at n = 8, 9, and 10 are almost the same (±0.1 eV),[19b] implying that the energetics

dx.doi.org/10.1021/ja311695t | J. Am. Chem. Soc. 2013, 135, 2991−2998

shown in Figure 4b for reaction of $Ti_8O_{17}^-$ + CO may be adaptable to larger reaction systems $(TiO_2)_nO^-$ + CO ($n > 8$).

For zirconium system, the fourth column of Table 1 tells that the large CO_2 desorption energy ($\Delta H_{D\text{-}CO2}$) decreases by only 0.22 eV as cluster size increases from $n = 3$ to 7. The $\Delta H_{D\text{-}CO2}$ value is increased to 1.30 eV at $n = 8$, which can be due to a large structural change of $(ZrO_2)_nO^-$ at $n = 7 \rightarrow 8$: the $(ZrO_2)_n$ moiety at $n = 8$ has no Zr−O terminal bonds and becomes compact (Figure 3; see also ref 36a). The big difference of the CO_2 desorption energy (0.13 versus 1.30 eV) from the large titanium and zirconium oxide cluster systems implies that bulk titania and zirconia can be quite different in terms of CO oxidation.

4.2. A Correlation with the Condensed Phase System. The titanium and zirconium oxide cluster anions with dimensions up to a nanosize may well be used to mimic the negatively charged oxide supports than can be generated from charge transfer[16] within the Au/TiO_2 and Au/ZrO_2 catalysts. It has been evidenced that in the oxidation of CO over Au/TiO_2 and related catalysts, the oxide supports participate directly in the reaction by supplying active oxygen species at the perimeter of the gold−oxide interface.[4] In addition, the Au/TiO_2 and Au/ZrO_2 catalysts behave quite differently in the CO oxidation.[2,4b,5] Thus, on the basis of the present findings we propose a fundamental mechanistic difference between the Au/TiO_2 and Au/ZrO_2 catalysts with regard to low-temperature CO oxidation (Figure 5). For the former system the reaction of CO

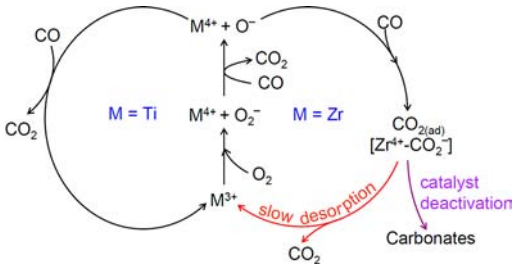

Figure 5. Proposed catalytic cycles involving O_2^- and O^- radicals for low-temperature CO oxidation over titania (left) and zirconia (right) supported gold. Gold may participate in the O−O bond activation (reaction 1 and Figure S19, Supporting Information).

with the O^- radical anions (generated from reaction 1) does not proceed through the long-lived surface-adsorbed CO_2. This feature is reserved for the zirconium system.

Of course, the gas-phase cluster and condensed phase surface reactions can differ substantially. To begin with, in the gas phase the energy released in bond formation is not quickly dissipated to the environment; thus, small cluster systems increase their effective temperature.[40] Nevertheless, the insight provided by the gas phase cluster study may well be useful to interpret surface reactions. The fifth and sixth columns of Table 2 indicate that CO_2 desorption over bulk surfaces at room temperature and below (230 K) can be very fast for the titanium and rather sluggish for the zirconium systems. As a result, surface adsorbed CO_2 (or CO_2^-) over zirconia at low temperature can desorb into gas-phase CO_2 only inefficiently; consequently, deactivation of the catalyst due to the occupation of the catalytically active sites may occur as the generated CO_2^- can react with O^{2-} [$CO_2^- + O^{2-} + M^{x+} \rightarrow CO_3^{2-} + M^{(x-1)+}$][41] and accumulates to form surface carbonates (Figure 5, right cycle).

The comparative studies of Konova et al. on Au/TiO_2[2] and Au/ZrO_2[5] catalysts for CO oxidation indicate that the two catalysts are active at temperatures down to 213 and 230 K, respectively. Moreover, the Au/TiO_2 catalyst is apparently more active and more stable than Au/ZrO_2. For example, at room temperature, the CO conversion >90% lasts for 150 min for Au/TiO_2 while the initial CO conversion of only 83% on Au/ZrO_2 is followed by a quick deactivation of the catalyst (within 50 min). Through carbon balance analysis, the adsorption of CO and its accumulation as carbonates have been proposed as a major reason for the deactivation of Au/ZrO_2.[5] The mechanism proposed in Figure 5, involving O_2^- and O^- radicals, is not only in line with the observed activity of both Au/TiO_2 and Au/ZrO_2 for the low-temperature CO oxidation; more importantly, it also rationalizes why the former system is superior to the latter.

Further support for the mechanisms depicted in Figure 5 comes from a different corner. In a recent study[4a] employing the technique of temporal analysis of products (TAP, at T = 418 K) and using the isotope switching method, for the Au/ZrO_2 catalyst it was shown that, starting with ^{13}CO, one detects $^{13}CO_2$ products even 50 pulses (~30 min) after a switch to ^{12}CO, and the intensity of the $^{12}CO_2$ isotopomer increases only slowly and has not yet reached its final value even after 50 pulses. In sharp contrast, on the Au/TiO_2 catalyst, there is almost no build-up of carbon-containing surface species (CCSS) at the beginning, and the small amount of reversibly stored CCSS present during the reaction is exchanged completely within the first five pulses after the switch.[4a] The slow disappearance of $^{13}CO_2$ over Au/ZrO_2 in the TAP measurements corresponds to the "slow desorption" of CO_2 from zirconia as revealed by the present cluster study (Figure 5; see also the last column of Table 2).

The reactivity (reaction 4 versus 5) of the O^- radicals present in Ti and Zr oxide clusters correlates with the different behaviors of titania and zirconia supports in the catalytic CO oxidation. It is noteworthy that the ceria-supported gold catalyst also has a comparable, high activity as well as good stability for the low-temperature CO oxidation as the Au/TiO_2 does.[6] This is well-consistent with previous experiments that the reactions of $(CeO_2)_nO^-$ ($n = 4$−21) with CO follow the reactivity pattern of $(TiO_2)_nO^-$ (reaction 4) rather than that of $(ZrO_2)_nO^-$ (reaction 5).[42]

To further support the hypothesis (reactions 1 and 2) that an "atomic" oxygen radical anion is indeed involved in the low-temperature CO oxidation using Au/TiO_2 and closely related catalysts,[2−7] the mechanism of reaction 1 that involves the O−O bond activation is interpreted by a DFT study of CO oxidation by a model cluster HAu_2TiO_4 that contains a superoxide (O_2^-) and a metallic Au_2 unit. An overall barrierless pathway is obtained (Figure S19, Supporting Information), and the product HAu_2TiO_3 can contain the O^- radical anion, which is expected to react with another CO through reaction 2. One should be aware of the fact that the real Au/TiO_2 catalysts should be much more complex than HAu_2TiO_4, and further experimental and theoretical investigations on gold-doped titanium oxide clusters[19h] are important to discover the nature of gold in low-temperature CO oxidation. The study of titanium and zirconium oxide clusters free of gold in this work provides good evidence for involvement of atomic oxygen radical anions (Figure 5) in this important reaction, which can be a good clue for future investigations.

5. CONCLUSIONS

The reactions of two series of cluster anions $(TiO_2)_nO^-$ and $(ZrO_2)_nO^-$ with CO have been studied by mass spectrometry (n = 3−25) and density functional theory calculations (n = 3−8). The atomic radical anions (O^-) bound to the clusters oxidize CO to form free CO_2 and cluster surface adsorbed CO_2 in the titanium and zirconium reaction systems, respectively. The different reactivity correlates with the difference in the orbital energies of titanium 3d versus zirconium 4d, as one d orbital accepts the electron from the net reaction CO + $(O^-)_{ad}$ → CO_2 + $(e^-)_{ad}$ in each cluster system. The energy required for desorption of CO_2 from the CO oxidatively absorbed intermediate $(MO_2)_nOCO^-$ decreases significantly as the cluster size (n) increases for the titanium (M = Ti) system while such an energy variation is not apparent for zirconium (M = Zr) counterpart. The reactivity pattern of the O^- bonded $(TiO_2)_nO^-$ and $(ZrO_2)_nO^-$ correlates very well with different behaviors of titania and zirconia supports in the low-temperature catalytic CO oxidation, which provides good evidence that the atomic oxygen radical anions are involved in this important catalytic reaction. Further, the reaction of CO with O^- plays an important role because desorption of the reaction product (CO_2) is directly associated with the regeneration or the deactivation of the catalyst, being strongly dependent on the nature of the oxide supports. This insight represents an important step toward a better mechanistic understanding of the low-temperature CO oxidation as well as the nature of atomic oxygen radical anions on oxide-based catalysts in general.

■ ASSOCIATED CONTENT

Supporting Information

Interactions of CO with metal atoms in the oxide clusters, an interpretation of the DFT-calculated electron affinities of $(TiO_2)_n$ and $(ZrO_2)_n$, additional TOF mass spectra and DFT calculated results, and the complete ref 22. This material is available free of charge via the Internet at http://pubs.acs.org.

■ AUTHOR INFORMATION

Corresponding Author

shengguihe@iccas.ac.cn

Notes

The authors declare no competing financial interest.

■ ACKNOWLEDGMENTS

This work is supported by Chinese Academy of Sciences (Knowledge Innovation Program KJCX2-EW-H01, CMS-PY-201202), the National Natural Science Foundation of China (Nos. 20933008 and 21173233), Major Research Plan of China (Nos. 2011CB932302 and 2013CB834603), and the China Postdoctoral Science Foundation (No. 2012T50138). We thank Prof. Helmut Schwarz for reading and improving the original manuscript.

■ REFERENCES

(1) (a) Min, B. K.; Friend, C. M. *Chem. Rev.* **2007**, *107*, 2709−2724. (b) Xie, X. W.; Li, Y.; Liu, Z. Q.; Haruta, M.; Shen, W. J. *Nature* **2009**, *458*, 746−749. (c) Freund, H. J.; Meijer, G.; Scheffler, M.; Schlogl, R.; Wolf, M. *Angew. Chem., Int. Ed.* **2011**, *50*, 10064−10094. (d) Royer, S.; Duprez, D. *ChemCatChem* **2011**, *3*, 24−65.

(2) Konova, P.; Naydenov, A.; Venkov, Cv.; Mehandjiev, D.; Andreeva, D.; Tabakova, T. *J. Mol. Catal. A: Chem.* **2004**, *213*, 235−240.

(3) (a) Haruta, M.; Yamada, N.; Kobayashi, T.; Iijima, S. *J. Catal.* **1989**, *115*, 301−309. (b) Bond, G. C.; Louis, C.; Thompson, D. T. *Catalysis by Gold*; Imperial College Press: London, 2006; pp 176−180.

(4) (a) Kotobuki, M.; Leppelt, R.; Hansgen, D. A.; Widmann, D.; Behm, R. J. *J. Catal.* **2009**, *264*, 67−76. (b) Widmann, D.; Liu, Y.; Schüth, F.; Behm, R. J. *J. Catal.* **2010**, *276*, 292−305. (c) Widmann, D.; Behm, R. J. *Angew. Chem., Int. Ed.* **2011**, *50*, 10241−10245.

(5) Konova, P.; Naydenov, A.; Tabakova, T.; Mehandjiev, D. *Catal. Commun.* **2004**, *5*, 537−542.

(6) (a) Carrettin, S.; Concepción, P.; Corma, A.; Nieto, J. M. L.; Puntes, V. F. *Angew. Chem., Int. Ed.* **2004**, *43*, 2538−2540. (b) Guzman, J.; Carrettin, S.; Fierro-Gonzalez, J. C.; Hao, Y. L.; Gates, B. C.; Corma, A. *Angew. Chem., Int. Ed.* **2005**, *44*, 4778−4781.

(7) Liu, H.; Kozlov, A. I.; Kozlova, A. P.; Shido, T.; Asakura, K.; Iwasawa, Y. *J. Catal.* **1999**, *185*, 252−264.

(8) Fu, Q.; Saltsburg, H.; Flytzani-Stephanopoulos, M. *Science* **2003**, *301*, 935−938.

(9) (a) Che, M.; Tench, A. J. *Adv. Catal.* **1982**, *31*, 77−133. (b) Panov, G. I.; Dubkov, K. A.; Starokon, E. V. *Catal. Today* **2006**, *117*, 148−155. (c) Note that O^- is often termed as an oxygen-centered radical and labeled as $O^{\bullet-}$ or $O^{-\bullet}$ in the literature.

(10) Note that it was identified that O_2^- is unable to react with CO in the absence of gold at low-temperature.[6,7]

(11) (a) O'Hair, R. A. J.; Khairallah, G. N. *J. Cluster Sci.* **2004**, *15*, 331−363. (b) Böhme, D. K.; Schwarz, H. *Angew. Chem., Int. Ed.* **2005**, *44*, 2336−2354. (c) Schröder, D.; Schwarz, H. *Proc. Natl. Acad. Sci. U. S. A.* **2008**, *105*, 18114−18119. (d) Gong, Y.; Zhou, M. F.; Andrews, L. *Chem. Rev.* **2009**, *109*, 6765−6808. (e) Roithová, J.; Schröder, D. *Chem. Rev.* **2010**, *110*, 1170−1211. (f) Zhai, H. J.; Wang, L. S. *Chem. Phys. Lett.* **2010**, *500*, 185−195. (g) Castleman, A. W., Jr. *Catal. Lett.* **2011**, *141*, 1243−1253. (h) Zhao, Y. X.; Wu, X. N.; Ma, J. B.; He, S. G.; Ding, X. L. *Phys. Chem. Chem. Phys.* **2011**, *13*, 1925−1938. (i) Yin, S.; Bernstein, E. R. *Int. J. Mass. Spectrom.* **2012**, *321*−*322*, 49−65. (j) Lang, S. M.; Bernhardt, T. M. *Phys. Chem. Chem. Phys.* **2012**, *14*, 9255−9269. (k) Asmis, K. R. *Phys. Chem. Chem. Phys.* **2012**, *14*, 9270−9281.

(12) (a) Dong, F.; Heinbuch, S.; Xie, Y.; Rocca, J. J.; Bernstein, E. R.; Wang, Z. C.; Deng, K.; He, S. G. *J. Am. Chem. Soc.* **2008**, *130*, 1932−1943. (b) Nößler, M.; Mitrić, R.; Koutecký, V. B.; Johnson, G. E.; Tyo, E. C.; Castleman, A. W., Jr. *Angew. Chem., Int. Ed.* **2010**, *49*, 407−410. (c) Schwarz, H. *Angew. Chem., Int. Ed.* **2011**, *50*, 10096−10115. (d) Ding, X. L.; Wu, X. N.; Zhao, Y. X.; He, S. G. *Acc. Chem. Res.* **2012**, *45*, 382−390. (e) Wu, X. N.; Xu, B.; Meng, J. H.; He, S. G. *Int. J. Mass Spectrom.* **2012**, *310*, 57−64. (f) Dietl, N.; Schlangen, M.; Schwarz, H. *Angew. Chem., Int. Ed.* **2012**, *51*, 5544−5555.

(13) Zhao, C.; Wachs, I. E. *Catal. Today* **2006**, *118*, 332−343.

(14) Lee, J.; Grabowski, J. J. *Chem. Rev.* **1992**, *92*, 1611−1647.

(15) Given the densities of bulk TiO_2 (4.23 g/cm^3) and ZrO_2 (5.68 g/cm^3), particles (round balls) with 1 nm diameter correspond to $(TiO_2)_{17}$ and $(ZrO_2)_{15}$ clusters.

(16) Manzoli, M.; Boccuzzi, F.; Chiorino, A.; Vindigni, F.; Deng, W.; Flytzani-Stephanopoulos, M. *J. Catal.* **2007**, *245*, 308−315.

(17) (a) Grunwaldt, J. D.; Maciejewski, M.; Becker, O. S.; Fabrizioli, P.; Baiker, A. *J. Catal.* **1999**, *186*, 458−469. (b) Arrii, S.; Morfin, F.; Renouprez, A. J.; Rousset, J. L. *J. Am. Chem. Soc.* **2004**, *126*, 1199−1205. (c) Comotti, M.; Li, W. C.; Spliethoff, B.; Schüth, F. *J. Am. Chem. Soc.* **2006**, *128*, 917−924.

(18) (a) Tyo, E. C.; Nössler, M.; Mitrić, R.; Bonačić-Koutecký, V.; Castleman, A. W., Jr. *Phys. Chem. Chem. Phys.* **2011**, *13*, 4243−4249. (b) Johnson, G. E.; Mitrić, R.; Nössler, M.; Tyo, E. C.; Bonačić-Koutecký, V.; Castleman, A. W., Jr. *J. Am. Chem. Soc.* **2009**, *131*, 5460−5470. (c) Johnson, G. E.; Mitrić, R.; Tyo, E. C.; Bonačić-Koutecký, V.; Castleman, A. W., Jr. *J. Am. Chem. Soc.* **2008**, *130*, 13912−13920.

(19) (a) Hamad, S.; Catlow, C. R. A.; Woodley, S. M.; Lago, S.; Mejias, J. A. *J. Phys. Chem. B* **2005**, *109*, 15741−15748. (b) Zhai, H. J.; Wang, L. S. *J. Am. Chem. Soc.* **2007**, *129*, 3022−3026. (c) Calatayud, M.; Minot, C. *J. Phys. Chem. C* **2009**, *113*, 12186−12194. (d) Qu, Z. W.; Zhu, H. *J. Comput. Chem.* **2010**, *31*, 2038−2045. (e) Li, S.; Dixon,

D. A. *J. Phys. Chem. A* **2010**, *114*, 2665−2683. (f) Woodley, S. M.; Hamad, S.; Catlow, C. R. A. *Phys. Chem. Chem. Phys.* **2010**, *12*, 8454−8465. (g) Janssens, E.; Santambrogio, G.; Brümmer, M.; Wöste, L.; Lievens, P.; Sauer, J.; Meijer, G.; Asmis, K. R. *Phys. Rev. Lett.* **2006**, *96*, 233401(4). (h) Himeno, H.; Miyajima, K.; Yasuike, T.; Mafuné, F. *J. Phys. Chem. A* **2011**, *115*, 11479−11485. (i) von Helden, G.; Kirilyuk, A.; van Heijnsbergen, D.; Sartakov, B.; Duncan, M. A.; Meijer, G. *Chem. Phys.* **2000**, *262*, 31−39. (j) Matsuda, Y.; Shin, D. N.; Bernstein, E. R. *J. Chem. Phys.* **2004**, *120*, 4142−4149.

(20) (a) Ma, J. B.; Wu, X. N.; Zhao, Y. X.; Ding, X. L.; He, S. G. *J. Phys. Chem. A* **2010**, *114*, 10024−10027. (b) Wu, X. N.; Ma, J. B.; Xu, B.; Ding, X. L.; He, S. G. *J. Phys. Chem. A* **2011**, *115*, 5238−5246.

(21) (a) Becke, A. D. *J. Chem. Phys.* **1993**, *98*, 5648−5652. (b) Lee, C. T.; Yang, W. T.; Parr, R. G. *Phys. Rev. B* **1988**, *37*, 785−789.

(22) Frisch, M. J. et al. *Gaussian 03*, Revision C.02, Gaussian, Inc.: Wallingford, CT, 2004.

(23) Sierka, M.; Döbler, J.; Sauer, J.; Santambrogio, G.; Brümmer, M.; Wöste, L.; Janssens, E.; Meijer, G.; Asmis, K. R. *Angew. Chem., Int. Ed.* **2007**, *46*, 3372−3375.

(24) Hay, P. J.; Wadt, W. R. *J. Chem. Phys.* **1985**, *82*, 270−283.

(25) Schäfer, A.; Huber, C.; Ahlrichs, R. *J. Chem. Phys.* **1994**, *100*, 5829−5835.

(26) Andrae, D.; Häussermann, U.; Dolg, M.; Stoll, H.; Preuss, H. *Theor. Chim. Acta* **1990**, *77*, 123−141.

(27) Schlegel, H. B. *J. Comput. Chem.* **1982**, *3*, 214−218.

(28) (a) Gonzalez, C.; Schlegel, H. B. *J. Chem. Phys.* **1989**, *90*, 2154−2161. (b) Gonzalez, C.; Schlegel, H. B. *J. Phys. Chem.* **1990**, *94*, 5523−5527.

(29) Steinfeld, J. I.; Francisco, J. S.; Hase, W. L. *Chemical Kinetics and Dynamics*; Prentice Hall: Upper Saddle River, NJ, 1999; pp 313−314.

(30) Beyer, T.; Swinehart, D. R. *ACM Commun.* **1973**, *16*, 379.

(31) Xue, W.; Wang, Z. C.; He, S. G.; Xie, Y.; Bernstein, E. R. *J. Am. Chem. Soc.* **2008**, *130*, 15879−15888.

(32) (a) Dong, F.; Heinbuch, S.; He, S. G.; Xie, Y.; Rocca, J. J.; Bernstein, E. R. *J. Chem. Phys.* **2006**, *125*, 164318(8). (b) Wang, W. G.; Wang, Z. C.; Yin, S.; He, S. G.; Ge, M. F. *Chin. J. Chem. Phys.* **2007**, *20*, 412−418. (c) Yin, S.; Xue, W.; Ding, X. L.; Wang, W. G.; He, S. G.; Ge, M. F. *Int. J. Mass Spectrom.* **2009**, *281*, 72−78. (d) Li, X. N.; Xu, B.; Ding, X. L.; He, S. G. *Dalton Trans.* **2012**, *41*, 5562−5570. (e) Ma, J. B.; Zhao, Y. X.; He, S. G.; Ding, X. L. *J. Phys. Chem. A* **2012**, *116*, 2049−2054.

(33) Kummerlöwe, G.; Beyer, M. K. *Int. J. Mass Spectrom.* **2005**, *244*, 84−90.

(34) (a) Su, T.; Bowers, M. T. *J. Chem. Phys.* **1973**, *58*, 3027−3037. (b) Su, T.; Bowers, M. T. *Int. J. Mass Spectrom. Ion Phys.* **1973**, *12*, 347−356. (c) Su, T.; Bowers, M. T. *J. Am. Chem. Soc.* **1973**, *95*, 1370−1373.

(35) Zhao, Y. X.; Ding, X. L.; Ma, Y. P.; Wang, Z. C.; He, S. G. *Theor. Chem. Acc.* **2010**, *127*, 449−465.

(36) (a) The $(TiO_2)_n$ and $(ZrO_2)_n$ clusters have identical topological stucutures at n = 3, 6, and 7 (Figures S15 and S16, Supporting Information), while the EA of the small system (n = 3) is only slightly higher for Ti versus Zr species (the sixth column of Table 1). This is in contrast to the fact that the energy of Ti 3d orbital can be significantly lower than that of Zr 4d orbital (by 0.66 eV under the approximation of H orbital energies). Moreover, the experimental EA of ZrO_2 was determined to be 1.64 ± 0.03 eV[36b] which is even higher than that of TiO_2 (1.59 ± 0.03 eV).[36c] The EA values in the sixth column of Table 1 are also strongly dependent on the cluster size: 4.78 eV at n = 8 versus 3.10 eV at n = 3 for the Ti system and 2.05 eV at n = 8 versus 3.34 eV at n = 6 for the Zr system. As a result, to further understand the EAs of $(TiO_2)_n$ versus $(ZrO_2)_n$ clusters, one should consider other factors in addition to the relative energy of atomic orbitals (3d versus 4d or 5s versus 6s for n = 1 system[36b]). It turns out that the size-dependent EAs of $(MO_2)_n$ clusters (M = Ti, Zr; n = 3−8) can be well-interpreted on the basis of the orbital interactions between the Nd_{z^2} (N = 3 for Ti and N = 4 for Zr) and the 2p orbitals of the neighboring oxygen atoms. An interpretation of DFT-calculated EA values can be found in the Supporting Information. (b) Zheng, W. J.; Bowen, K. H., Jr.; Li, J.; Dabkowska, I.; Gutowski, M. *J. Phys. Chem. A* **2005**, *109*, 11521−11525. (c) Wu, H. B.; Wang, L. S. *J. Chem. Phys.* **1997**, *107*, 8221−8228.

(37) The reactions of $(ZrO_2)_{3,4}O^-$ with CO under single collision conditions (no bath gas cooling) generates $(ZrO_2)_{3,4}^-$; see ref 18b.

(38) (a) Justes, D. R.; Mitrić, R.; Moore, N. A.; Bonačić-Koutecký, V.; Castleman, A. W., Jr. *J. Am. Chem. Soc.* **2003**, *125*, 6289−6299. (b) Feyel, S.; Döbler, J.; Schröder, D.; Sauer, J.; Schwarz, H. *Angew. Chem., Int. Ed.* **2006**, *45*, 4681−4681. (c) Ding, X. L.; Zhao, Y. X.; Wu, X. N.; Wang, Z. C.; Ma, J. B.; He, S. G. *Chem.—Eur. J.* **2010**, *16*, 11463−11470. (d) Zhao, Y. X.; Wu, X. N.; Wang, Z. C.; He, S. G.; Ding, X. L. *Chem. Commun.* **2010**, *46*, 1736−1738. (e) Ding, X. L.; Wu, X. N.; Zhao, Y. X.; Ma, J. B.; He, S. G. *ChemPhysChem* **2011**, *12*, 2110−2117. (f) Ma, J. B.; Wang, Z. C.; Schlangen, M.; He, S. G.; Schwarz, H. *Angew. Chem., Int. Ed.* **2012**, *51*, 5991−5994.

(39) (a) Fialko, E. F.; Kikhtenko, A. V.; Goncharov, V. B.; Zamaraev, K. I. *J Phys. Chem. A* **1997**, *101*, 8607−8613. (b) Johnson, G. E.; Tyo, E. C.; Castleman, A. W., Jr. *Proc. Natl. Acad. Sci. U. S. A.* **2008**, *105*, 18108−18113. (c) Wu, X. N.; Zhao, Y. X.; Xue, W.; Wang, Z. C.; He, S. G.; Ding, X. L. *Phys. Chem. Chem. Phys.* **2010**, *12*, 3984−3997. (d) Wang, Z. C.; Dietl, N.; Kretschmer, R.; Weiske, T.; Schlangen, M.; Schwarz, H. *Angew. Chem., Int. Ed.* **2011**, *50*, 12351−12354. (e) Schlangen, M.; Schwarz, H. *Catal. Lett.* **2012**, *142*, 1265−1278.

(40) Bondybey, V. E.; Beyer, M. K. *J. Phys. Chem. A* **2001**, *105*, 951−960.

(41) Xu, B.; Zhao, Y. X.; Ding, X. L.; He, S. G. *Int. J. Mass Spectrom.* **2012**, *334*, 1−7.

(42) Wu, X. N.; Ding, X. L.; Bai, S. M.; Xu, B.; He, S. G.; Shi, Q. *J. Phys. Chem. C* **2011**, *115*, 13329−13337.